

Sn(II)-containing phosphates as optoelectronic materials

Qiaoling Xu,¹ Yuwei Li,² Lijun Zhang,^{1,*} Weitao Zheng,¹ David J. Singh,^{2,1,†} and Yanming Ma^{3,‡}

¹College of Materials Science and Engineering and Key Laboratory of Automobile Materials of MOE, Jilin University, Changchun 130012, China

²Department of Physics and Astronomy, University of Missouri, Columbia, MO 65211-7010 USA

³State Key Laboratory of Superhard Materials, Jilin University, Changchun 130012, China

(Dated: October 9, 2018)

We theoretically investigate Sn(II) phosphates as optoelectronic materials using first principles calculations. We focus on known prototype materials $\text{Sn}_n\text{P}_2\text{O}_{5+n}$ ($n=2, 3, 4, 5$) and a previously unreported compound, SnP_2O_6 ($n=1$), which we find using global optimization structure prediction. The electronic structure calculations indicate that these compounds all have large band gaps above 3.2 eV, meaning their transparency to visible light. Several of these compounds show relatively low hole effective masses ($\sim 2\text{-}3 m_0$), comparable the electron masses. This suggests potential bipolar conductivity depending on doping. The dispersive valence band-edges underlying the low hole masses, originate from the anti-bonding hybridization between the Sn 5s orbitals and the phosphate groups. Analysis of structure-property relationships for the metastable structures generated during structure search shows considerable variation in combinations of band gap and carrier effective masses, implying chemical tunability of these properties. The unusual combinations of relatively high band gap, low carrier masses and high chemical stability suggests possible optoelectronic applications of these Sn(II) phosphates, including *p-type* transparent conductors. Related to this, calculations for doped material indicate low visible light absorption, combined with high plasma frequencies.

I. INTRODUCTION

Materials for optoelectronic application must have a suitable combination of optical properties, including band gap, and electronic properties, such as mobility and dopability. A particularly important class of optoelectronic materials are the transparent conductors. High performance *n-type* transparent conducting oxides (TCOs) are known, including Sn doped In_2O_3 (ITO). The best *p-type* TCOs have inferior performance due to lower mobility and higher optical absorption [1, 2]. The difficulties in realizing high-performance *p-type* TCOs include the rather localized O *p* derived valence bands of most oxides. The valence bands then have heavy effective masses and low hole mobilities. Furthermore, oxide chemistry strongly favors an O^{2-} valence leading to low energy deep defect levels that prevent high *p-type* carrier concentrations. These difficulties suggest the exploration of alternate chemistries to find new optoelectronic materials.

One approach is to take advantage of the coupling/hybridization between O *p* and states from other atoms, as exemplified by delafossite CuAlO_2 . In that Cu^{1+} compound the valence band edge has substantial Cu *d* character. The hybridization between the Cu *d* and O *p* states improves the dispersion of the valence bands, while the chemical tendency of Cu to favor higher valence states, e.g. Cu^{2+} enables heavy *p-type* doping [3]. The effective mass of CuAlO_2 is reported as $m^*=2.6 m_0$, comparable to other *p-type* TCO materials, e.g. SrCu_2O_2 ,

with $m^*=2.1 m_0$ and ZnRh_2O_4 , with $m^*=3.4 m_0$. [4, 5]. SnO , which has a band gap somewhat to small to be a good TCO in the visible, has a hole density of states effective mass $m^*=0.9 m_0$. [6] Nonetheless, the lower dispersion of the valence bands of CuAlO_2 relative to the conduction bands of ITO leads to a large number of bands below the valence band maximum (VBM) including the 1-3 eV binding energy range. When doped, optical transitions from these bands to the empty states at the valence band maximum can degrade the transparency. A similar strategy has been used with certain non-transition metal elements where the VBM can be from hybridized metal *s* - O *p* combinations. These include low-valence state cations of group III, IV, V metals (for instance Sn^{+2} , Pb^{+2} , Bi^{+3} , Tl^{+} , etc.). An example is the SnO binary compound [7] (n.b., Sn compounds are particularly attractive because Sn is a relatively low cost, benign ingredient). Ternary phases have also been studied, with promising results both for transparent conducting and electronic application. [8, 9] Theoretical work has mainly emphasized finding suitable combinations of band gap and hole effective mass [4].

Here we explore a different class of materials, specifically metal phosphate compounds, using Sn(II) phosphates as a first example (here we refer to both ortho- and pyro-phosphates generically as phosphates). We investigate band gap and effective mass, as well as the optical properties when doped. The rationale is that the phosphates have very stable phosphate polyanions that may provide good transport along the anion backbone and are based on Zintl chemistry, that may facilitate realization of a large number of compounds from which to select and may additionally provide enough flexibility to enable doping. The stability of phosphates is key to many of their applications, including waste storage

* Corresponding author: lijun_zhang@jlu.edu.cn

† Corresponding author: singhdj@missouri.edu

‡ Corresponding author: mym@jlu.edu.cn

forms [10–12], catalysts [13, 14], bonding agents in refractory and other ceramics [15], laser glass for very high power lasers [16], battery materials [17, 18], biological processes [19], and others. It is also noteworthy that phosphates can have significant electronic activity, as in catalysis, energy transport in scintillators, [20, 21] and in biology. This further motivates the present work. Specifically, the large phosphate anions that can form strongly bonded networks suggests the possibility of charge transport. Furthermore, metal vacancies would be expected to *p-type* dopants in these compounds, while the very high chemical stability of the phosphate polyanions could prevent the formation of compensating defects on the polyanion lattice. However, we note that there has to date been very limited investigation of phosphates as electronic materials [22].

The main valence bands of these phosphates come from the bonding states of the phosphate backbone, while the conduction bands come from metal states that lie in the large gap between the bonding and antibonding states of the phosphate groups [23]. In the case of Sn(II), the low valence state of Sn suggests the possibility that Sn *s* states may also occur at or near the VBM, which could provide additional connectivity between the phosphate groups and improve *p-type* conduction. As discussed below, we do find that the Sn *s* states in these compounds occur at the top of the valence bands, so that the VBM has predominant Sn *s* character.

Key initial questions to address are whether Sn(II) phosphates will have suitable gaps, whether any compounds exist that have sufficient connection between the phosphate units to enable light valence band masses and whether other properties are consistent with *p-type* optoelectronic applications, especially *p-type* transparent conducting behavior. It is also of interest to explore the range of properties that can be realized, as applications will no doubt benefit from chemical tuning [22].

A series of stoichiometric Sn(II) phosphate compounds have been reported experimentally. Here we initially focus on a group of prototype materials, $\text{Sn}_n\text{P}_2\text{O}_{5+n}$ ($n=2, 3, 4, 5$) (Fig. 1). For $n=2$, there are two phases: a high-temperature α -phase and a room-temperature β -phase. We also performed structure searches for better connected Sn(II) phosphates ($n=1$), using the principle of obtaining better connectivity by choosing a stoichiometry that is expected to favor longer pyrophosphate chains. We note that such pyrophosphates also form glasses, often with properties similar to the corresponding crystalline phases, which may be advantageous for TCO applications, where amorphous phases such as IGZO (In-Ga-Zn-O) are useful [24, 25]. The high performance of amorphous IGZO shows that high degrees of crystalline perfection are not always needed in TCOs.

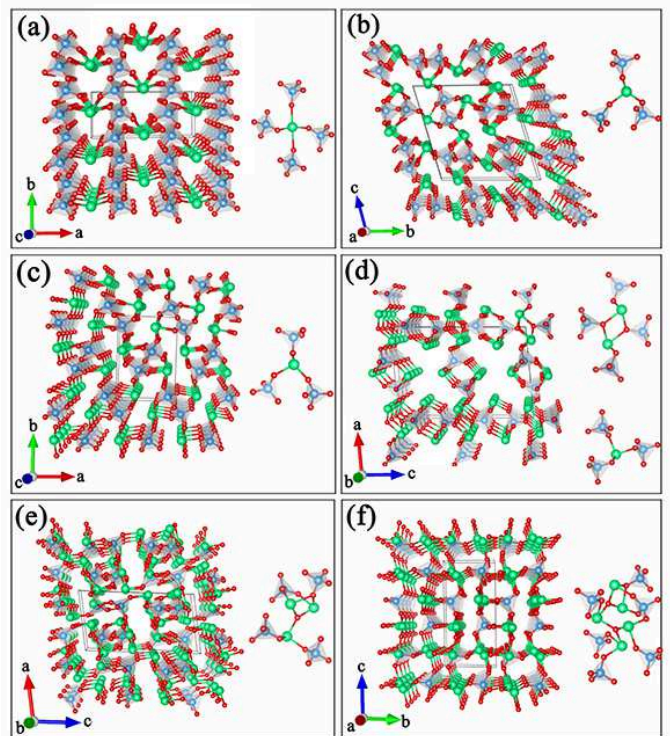


FIG. 1. Crystal structures of $\text{Sn}_n\text{P}_2\text{O}_{5+n}$ ($n=1, 2, 3, 4, 5$). (a) is for $n=1$, predicted stable configuration (with the symmetry Cc , $Z=4$). (b, c) is for $n=2$; the corresponding structures are the high-temperature α -phase (with the $P2_1/n$ symmetry, $Z=2$) and the room-temperature β -phase (with the $P\bar{1}$ symmetry, $Z=4$). (d, e, f) is for $n=3$ (with $P2_1/c$ symmetry, $Z=4$), $n=4$ (with the $P2_1/n$ symmetry, $Z=4$) and $n=5$ (with the symmetry $P\bar{1}$, $Z=2$), depicting the connections of the basic structural units. The Sn, P and O atoms are shown in green, blue, and red, respectively.

II. COMPUTATIONAL METHODS

The present calculations were done within density functional theory (DFT) using the Vienna ab initio software package (VASP) [26], with projector augmented-wave pseudopotentials. $2s^22p^4$, $5s^25p^2$ and $3s^23p^3$ valence state configurations for O, Sn and P, respectively, were used. We used the exchange correlation functional of Perdew, Burke and Ernzerhof (PBE) for the structure determinations [27, 28], in conjunction with an energy cutoff of 520 eV for the wave-function expansion and a grid spacing of $2\pi \times 0.04 \text{ \AA}^{-1}$ for Brillouin zone integration. The structures (including lattice parameters and internal atomic positions) are fully optimized via total energy minimization. (See supplementary information, Table S1 which shows the calculated lattice parameters in relation to experiment.)

The band gap plays a key role in optoelectronic materials. We used the modified Becke-Johnson (mBJ) potential [29] to calculate electronic structures and optical properties. In contrast to standard density functionals,

the mBJ potential gives band gaps in accord with experiment for most semiconductors and insulators that do not involve transition metal d or rare earth f derived levels [29–31]. As a test, we compared the electronic structures obtained with the mBJ potential to those obtained by the HSE06 [32, 33] hybrid functional method. (See supplementary information, Fig. S1, which shows the comparison between the mBJ and HSE06 band structures. As seen, they give almost identical band gaps and very similar band dispersion curves.) We also did tests comparing the electronic structures with all electron calculations performed with the general potential linearized augmented plane-wave (LAPW) method [34] using the mBJ [29] potential functional. We used the BoltzTraP code [35] to evaluate the effective transport masses for conductivity. These were determined by calculating the direction averaged σ/τ at a temperature of 300 K and the Fermi level set to the band edge. The mass is then given by the ratio of the number of carriers, n , over σ/τ (note that σ/τ is proportional to the square plasma frequency, i.e. the optical Drude n/m , which is the quantity relevant for electrical transport). As mentioned, we performed structure prediction calculations for SnP_2O_6 . These were done based on first principles DFT calculations combined with the particle swarm optimization algorithm as implemented in the CALYPSO code [36, 37]. We also particularly calculated the optical absorption spectra of the compounds when doped [38–40]. This is an important but often neglected aspect for identifying transparent conductors.

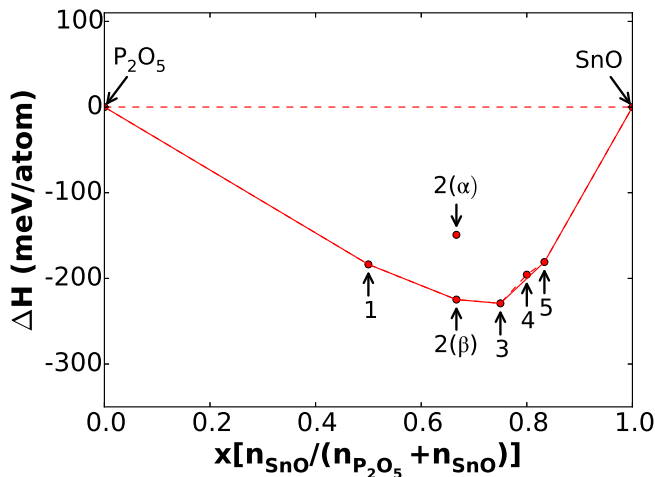


FIG. 2. Calculated formation enthalpies ΔH (in meV/atom), of various Sn(II) phosphates with respect to decomposition into the binary compounds, SnO and P_2O_5 . Note the large magnitudes of negative ΔH , consistent with the known generally high stability of metal phosphates.

III. RESULTS AND DISCUSSION

We begin with known compounds, $\text{Sn}_n\text{P}_2\text{O}_{5+n}$ ($n=2, 3, 4, 5$). As mentioned, $\text{Sn}_2\text{P}_2\text{O}_7$ shows two phases with a reversible structural transition at 623 K. These is a high temperature α -phase with spacegroup $P2_1/n$ and a β -phase, spacegroup $P\bar{1}$, obtained at room temperature [41]. Crystalline room-temperature phases of $\text{Sn}_3\text{P}_2\text{O}_8$ [42], $\text{Sn}_4\text{P}_2\text{O}_9$ and $\text{Sn}_5\text{P}_2\text{O}_{10}$ [43] have spacegroups $P2_1/c$, $P2_1/n$ and $P\bar{1}$, respectively. Fig. 2 shows their phase stability with respect to decomposition into the binary compounds SnO and P_2O_5 , using a convex hull plot. Except for α - $\text{Sn}_2\text{P}_2\text{O}_7$, which is the metastable phase stabilized at high temperature [41], all the materials show clear ($n=1, 2(\beta), 3, 5$) or marginal ($n=4$) thermodynamic stability against decomposition. This is in accord with experiment. Note that these compounds have large negative formation enthalpies, indicating their high chemical stabilities. As shown in Fig. 1, all of the compounds consist of PO_4 tetrahedra (joined by a corner shared O in the case of the pyrophosphates), and interstitial Sn, coordinated by the O of the phosphate anions. This type of structure reflects the very high stability of the phosphate and pyrophosphate anions.

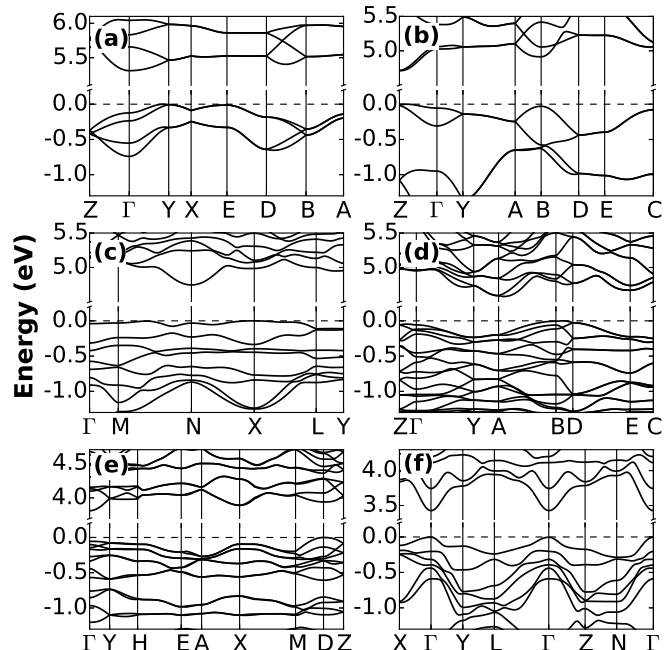


FIG. 3. Calculated band structures of $\text{Sn}_n\text{P}_2\text{O}_{5+n}$ (a ($n=1$), b ($n=2$ (α)), c ($n=2$ (β)), d ($n=3$), e ($n=4$), f ($n=5$)) using the mBJ potential.

Band structure plots are given in Fig. 3. The corresponding electronic densities of states (DOS) are given in Fig. 4. The valence bands are associated with the Sn 5s states, with anti-bonding hybridization of the phosphate groups. These Sn 5s states occur at the top of the valence bands, and at the very top the character is predominantly Sn s. Thus from the point of view of hole

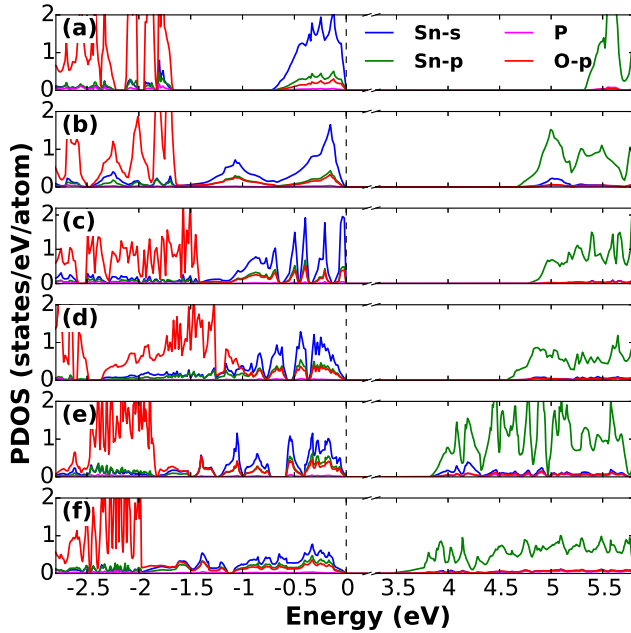


FIG. 4. Calculated projected densities of states (PDOS) for $\text{Sn}_n\text{P}_2\text{O}_{5+n}$ (a ($n=1$), b ($n=2$ (α)), c ($n=2$ (β)), d ($n=3$), e ($n=4$), f ($n=5$)). The blue, green, magenta, and red lines correspond to Sn s , Sn p , P (total), and O p states, respectively.

transport the Sn s orbitals link the phosphate groups, which can potentially form conducting channels.

We find that all compounds show large band gaps based on the mBJ calculations, as summarized in Fig. 5a. In particular, we obtain 5.31 eV for SnP_2O_6 (Fig. 3a) 4.64 eV and 4.74 eV for $\text{Sn}_2\text{P}_2\text{O}_7$ (α) and $\text{Sn}_2\text{P}_2\text{O}_7$ (β), respectively (Fig. 3b, 3c). The values are 4.55 eV, 3.81 eV, and 3.40 eV for $\text{Sn}_3\text{P}_2\text{O}_8$, $\text{Sn}_4\text{P}_2\text{O}_9$, and $\text{Sn}_5\text{P}_2\text{O}_{10}$, respectively (Fig. 3d, 3e, 3f). Interestingly, $\text{Sn}_5\text{P}_2\text{O}_{10}$ exhibits a direct band gap with a relatively small value compared to the other compounds. In any case, all these gaps are all well above the visible region and imply transparency to visible and in some cases near UV light for undoped materials. The calculated absorption spectra are shown in Fig. 7.

As mentioned, the valence band edges of the five compounds come from hybridization of Sn s and O p states associated with the phosphate anions (Fig. 4). The conduction bands are Sn p derived. As might be expected, the involvement of Sn s at the VBM leads to dispersive valence bands and thus lowers the effective mass of hole states. As shown in Fig. 5b, except for the case of $\text{Sn}_2\text{P}_2\text{O}_7$ (β), the effective masses of hole states (~ 2 -3 m_0) are comparable to those of electrons and are comparable to or even lower than most known p -type transparent conductors. We note that this combination of moderate effective mass for both holes and electrons, high band gap and high chemical stability is unusual.

The large hole effective mass of β phase $\text{Sn}_2\text{P}_2\text{O}_7$ comes from the very flat valence band edges (Fig. 3c).

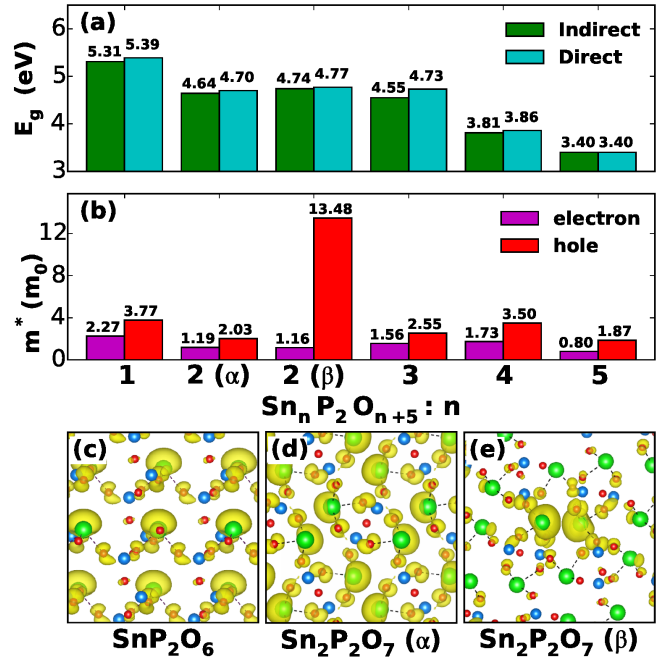


FIG. 5. The top panel shows the indirect and direct band gap for the $n=1, 2$ (α), 2 (β), $3, 4$ and 5 structures. Corresponding electron and hole effective masses are shown in b, respectively. Band decomposed charge density of valence-band top with isosurface level 0.002 for various configurations: $n=1, n=2$ (α) and $n=2$ (β), are plotted in the bottom panel. The color code: Sn green, P blue, O red.

The reason is seen in the character of the states forming the VBM. We show the band decomposed charge density of the valence-band edge states for the first three materials in Fig. 5b. The states around the valence-band edge for β phase of $\text{Sn}_2\text{P}_2\text{O}_7$ (Fig. 5e) come from Sn s orbitals without sufficient hybridization to the phosphate groups to produce dispersive bands.

In the binary compound, SnO, the hole effective mass shows strong anisotropy reflecting the layered structure [7]. This gives rise to strongly anisotropic hole transport behavior. This is also a characteristic of delafossite CuAlO_2 . While it is possible to make and use highly textured films, in general anisotropy is undesirable for applications. In the Sn(II) phosphates, the masses are more isotropic as seen from the band structures.

The calculated σ/τ (proportional to the square plasma frequency; τ is the relaxation time) as functions of carrier concentration are given in Fig. 6. For comparison, we also show results for a known p -type transparent conductor, delafossite CuAlO_2 . Conductivity of $\sim 1 \text{ Scm}^{-1}$ has been reported at doping levels of $1.3 \times 10^{17} \text{ cm}^{-3}$ for that material. [3] While the scattering rate will be important, we find that considering the band structure alone, the σ/τ for the compounds follows the order $\sigma(\text{Sn}_5\text{P}_2\text{O}_{10}) > \sigma(\text{Sn}_2\text{P}_2\text{O}_7(\alpha)) > \sigma(\text{Sn}_3\text{P}_2\text{O}_8) > \sigma(\text{Sn}_4\text{P}_2\text{O}_9) > \sigma(\text{CuAlO}_2) > \sigma(\text{SnP}_2\text{O}_6) > \sigma(\text{Sn}_2\text{P}_2\text{O}_7(\beta))$, suggesting that at least room temperature phase

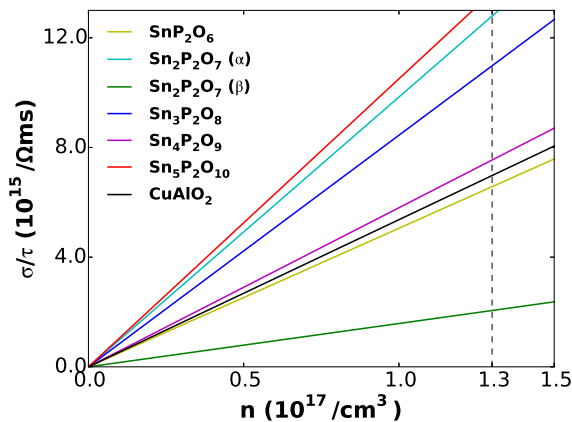


FIG. 6. The ratio of optical conductivities σ to the effective inverse scattering rate τ calculated for $n=1, 2(\alpha), 2(\beta), 3, 4, 5$ structures and CuAlO_2 , as a function of the carrier concentration. The reported experimental carrier concentration for high performance CuAlO_2 TCO is indicated by the dashed line.

$\text{Sn}_5\text{P}_2\text{O}_{10}$, $\text{Sn}_4\text{P}_2\text{O}_9$ and $\text{Sn}_3\text{P}_2\text{O}_8$, may be good conductors if doped, and that from an electronic point of view they may have performance comparable to or better than the delafossite.

We next consider interband transitions in doped material. This is a key ingredient in the performance of n -type TCOs. To address this important, but often neglected aspect, we calculate absorption spectra with virtual crystal doping. This allows transitions from lower bands into the now empty states at the top of the valence band [39, 40]. The calculated absorption spectra with p -type virtual crystal doping of 0.05 holes per Sn are shown in the inset of Fig. 7. Interestingly, there is an inverse Burstein-Moss shift with doping in which the apparent optical gap shrinks with hole doping. This reflects a downward shift of the Sn p derived conduction bands when holes are introduced into the Sn s derived valence band. This shift is larger than the lowering of the Fermi level with hole doping. Importantly, although there are interband transitions in the visible, we find that they are very weak, so that high transparency when doped is possible. This is a key requirement for a transparent conductor, and is not met for many materials with otherwise favorable gaps and effective masses.

An interesting question is whether increasing the length of the pyrophosphate chains will improve the properties by providing more connectivity in the polyanion lattice. To explore this issue we studied a lower O content composition, which would lead to longer chains, specifically, SnP_2O_6 (see Fig. 1a). We determined the crystal structure using the particle swarm optimization algorithms implemented in the CALYPSO code.

We began with a series of structural searches for the stoichiometric composition, SnP_2O_6 . The predicted lowest energy structures have Cc spacegroups, presented in

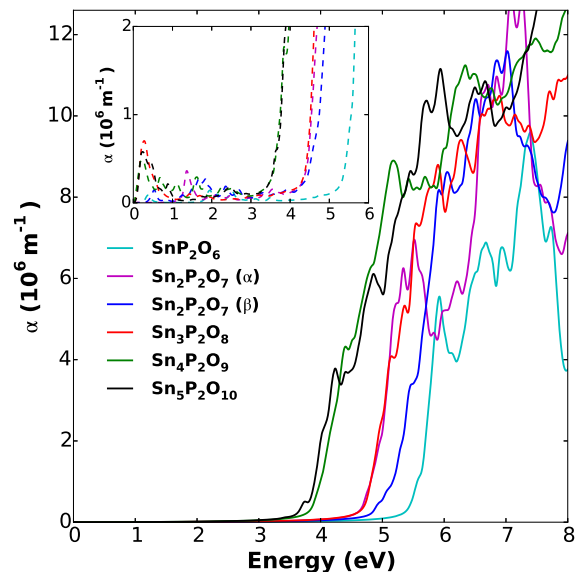


FIG. 7. Calculated absorption spectra for different compounds, $\text{Sn}_n\text{P}_2\text{O}_{5+n}$. The color information: cyan ($n=1$), magenta ($n=2$ (α)), blue ($n=2$ (β)), red ($n=3$), green ($n=4$), black ($n=5$). The dashed lines in the inset show the absorption spectra doping 0.05 holes per Sn. Note the low absorption in the visible (1.7 eV – 3.25 eV) even with heavy doping.

Fig. 1a (Supplementary information Table S2 gives the lattice constants and internal atomic coordinates). Note that this is a theoretically determined structure based on density functional calculations. This requires the use of finite cells, in the present case up to 18 atoms, with some calculations up to 36 atoms. It is possible that a more complex larger unit cell structure occurs; in that case the energy will be lower, and therefore the compound will still be stable. The predicted structure has Sn atoms coordinated by four O atoms to form square pyramids and $(\text{PO}_3)_n$ ($n \geq 2$) chains interconnected by corner shared P_2O_7 units. Importantly the result is a connected phosphate network with interstitial Sn cations.

We assessed the phase stability of the newly predicted SnP_2O_6 phase by using the standard thermodynamic stability analysis, as shown in Fig. 8. The experimentally known potentially competing compounds were considered. By analyzing the variation in chemical potentials of Sn and P, the predicted phase shows relatively large stable regions. In crystal growth, the thermodynamic equilibrium condition requires a stable SnP_2O_6 compound to meet the following three criteria:

$$\Delta\mu_{\text{Sn}} + 2\Delta\mu_{\text{P}} + 6\Delta\mu_{\text{O}} = \Delta H_f(\text{SnP}_2\text{O}_6), \quad (1)$$

$$\Delta\mu_I \leq 0, (I = \text{Sn}, \text{P}, \text{O}), \quad (2)$$

$$\begin{aligned} & n_i \Delta\mu_{Sn} + m_i \Delta\mu_P + q_i \Delta\mu_O \\ & \leq \Delta H_f(Sn_{n_i}P_{m_i}O_{q_i}), \quad i = 1, \dots, Z, \end{aligned} \quad (3)$$

where $\Delta\mu_I = \mu_i - \mu_i^0$ is the deviation of actual chemical potential of species i during growth (μ_i) from that of bulk elemental solid or gas phase (μ_i^0), and Z refers to the total number of competing phases. ΔH_f is the enthalpy of formation. Eq.(1) is for equilibrium growth. Eq.(2) is the actually allowed range of ΔH_f . Eq.(3) is for energetic stability against competing phases.

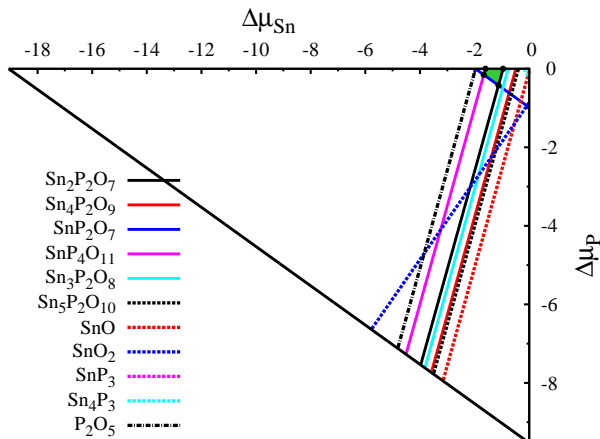


FIG. 8. Phase stability diagrams of SnP_2O_6 . Each line represents a known competing phase; the stable region for SnP_2O_6 is indicated in green.

Fig. 9 shows maps of the electron and hole effective mass *vs* band gap for the lowest energy metastable structures found in our structure search. Remarkably, different from many other families of materials the Sn(II) phosphates do not show a strong connection of mass and band gap. The implication is that this chemistry allows for flexible optimization of both gap and mass in connection with applications.

We calculated the electronic and optical properties of this SnP_2O_6 phase using the mBJ functional. Fig. 3a shows the band structure, which has an indirect band gap of 5.31 eV. The absorption spectrum shows a similar value for the optical gap (see Fig. 7). The band structure shows a gap from about -1.8 to -0.8 below the VBM. This gap separates the mainly Sn s derived bands making up the VBM from lower-lying mainly phosphate derived bands. We also find that the SnP_2O_6 structure shows reasonably low effective mass. For the Cc phase the hole and the electron effective masses are 3.77 m_0 and 2.27 m_0 , respectively. However, these numbers show that the hole mass of this more connected structure is not lower than the orthophosphate $\text{Sn}_3\text{P}_2\text{O}_8$, suggesting that the density of Sn atoms plays a more important role than the chain length in these Sn (II) phosphates.

We examined the low energy structures in terms of bond valence sums and other simple metrics, but did not

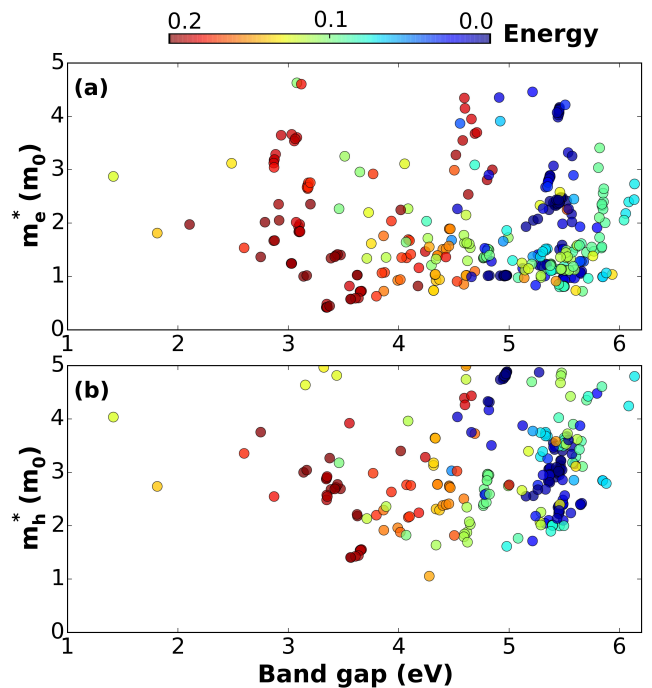


FIG. 9. Distribution map of the metastable compounds of SnP_2O_6 ($n=1$) with energies of no more than 0.2 eV/atom higher than the ground-state Cc structures, onto the variables of m_e^* vs band gap (a) and m_h^* vs band gaps (b), respectively. The RGB color bar represents range of energy from 0.0 eV/atom to 0.2 eV/atom.

find clear trends for the effective mass and band gap. We did find that the Sn bond valence sums for the low energy structures cluster near two and four, with the lowest energy structures having bond valence near two, as may be expected from the chemistry of Sn. We also find a common structural motif of phosphate chain structures, as may be anticipated from the known chemical stability of such polyanions. The key to our results is apparently the chemistry of Sn in a phosphate environment, where the Sn s states occur at the top of the valence band, leading to sizable band gaps governed by the splitting between the Sn s and Sn p levels. The hole effective mass is then controlled by the hopping in the Sn s derived valence bands. This certainly must depend on the detailed structure and in particular hopping assisted by the connectivity of the phosphate backbone, but also is favored by high Sn concentrations, which occur when the backbone is less connected.

IV. CONCLUSIONS

We report electronic structure calculations for some Sn(II) phosphates, in the context of optoelectronic applications. We find that these materials have large band gaps and at the same time still can have moderate effective masses for both holes and electrons. The bands near

the valence band maximum in all the compounds studied have Sn s character hybridized with states associated with the phosphate anions, while the conduction band is Sn p derived. Calculations of optical properties show that interband transitions in the visible are weak under hole doping. We also find an interesting inverse Burstein-Moss shift, which can be understood in terms of the Sn character of both the states at the valence band maximum and the conduction band minimum. Analysis of the metastable structures identified in a structure search suggests that the mass and band gap can be separately tuned in Sn(II) phosphates, in contrast to most other families of semiconductors. It will be of interest to determine whether these compounds can be doped, and also to examine other phosphate compounds as optoelectronic and electronic materials.

ASSOCIATED CONTENT

Supporting Information. Calculated electronic band structures of α -phase $\text{Sn}_2\text{P}_2\text{O}_7$ with different approaches; Theoretically optimized lattice parameters of $\text{Sn}_n\text{P}_2\text{O}_{5+n}$ ($n=2, 3, 4, 5$), compared with available experimental data. Detailed structural information for the newly predicted SnP_2O_6 .

ACKNOWLEDGMENTS

L.Z. acknowledges funding support from the Recruitment Program of Global Youth Experts in China. Some calculations were performed in the high performance computing center of Jilin University and on TianHe-1 (A) of the National Supercomputer Center in Tianjin. We acknowledge funding support from the National Key Laboratory of Shock Wave and Detonation Physics, National Natural Science Foundation of China (No.11534003), and National Key Research and Development Program of China (No. 2016YFB0201200).

-
- [1] D. S. Ginley and C. Bright, MRS Bulletin **25**, 15 (2000).
 [2] H. Kawazoe, H. Yanagi, K. Ueda, and H. Hosono, MRS Bulletin **25**, 28 (2000).
 [3] H. Kawazoe, M. Yasukawa, H. Hyodo, M. Kurita, H. Yanagi, and H. Hosono, Nature **389**, 939 (1997).
 [4] G. Hautier, A. Miglio, G. Ceder, G.-M. Rignanese, and X. Gonze, Nat. Commun. **4**, 2292 (2013).
 [5] R. Gillen and J. Robertson, Phys. Rev. B **84**, 035125 (2011).
 [6] H. Peng, A. Bikowski, A. Zakutayev, and S. Lany, APL Mater. **4**, 106103 (2016).
 [7] Y. Ogo, H. Hiramatsu, K. Nomura, H. Yanagi, T. Kamiya, M. Hirano, and H. Hosono, Appl. Phys. Lett. **93**, 032113 (2008).
 [8] H. J. Kim, U. Kim, H. M. Kim, T. H. Kim, H. S. Mun, B.-G. Jeon, K. T. Hong, W.-J. Lee, C. Ju, K. H. Kim, and K. Char, Appl. Phys. Express **5**, 061102 (2012).
 [9] S. A. Chambers, T. C. Kaspar, A. Prakash, G. Haugstad, and B. Jalan, Appl. Phys. Lett. **108**, 152104 (2016).
 [10] R. C. Ewing and L. Wang, Rev. Mineralogy Geochem. **48**, 673 (2002).
 [11] D. Day, Z. Wu, C. Ray, and P. Hrma, J. Non-Cryst. Sol. **241**, 1 (1998).
 [12] E. H. Oelkers and J.-M. Montel, Elements **4**, 113 (2008).
 [13] A. Clearfield and D. S. Thakur, Appl. Catalysis **26**, 1 (1986).
 [14] M. A. Banares, Catalysis Today **51**, 319 (1999).
 [15] W. D. KINGERY, J. Am. Ceram. Soc. **33**, 239 (1950).
 [16] J. Campbell and T. Suratwala, J. Non-Cryst. Sol. **263–264**, 318 (2000).
 [17] A. K. Padhi, K. Nanjundaswamy, and J. Goodenough, J. Electrochem. Soc. **144**, 1188 (1997).
 [18] X. Yu, J. Bates, G. Jellison, and F. Hart, J. Electrochem. Soc. **144**, 524 (1997).
 [19] F. H. Westheimer, Science **235**, 1173 (1987).
 [20] E. Nakazawa, J. Luminescence, **272** (1979).
 [21] A. Wojtowicz, D. Wenewski, A. Lempicki, and L. Boatner, Rad. Effects and Defects in Solids **135**, 305 (1995).
 [22] L. C. Lentz, B. Kolb, and A. M. Kolpak, Phys. Chem. Chem. Phys. **18**, 14122 (2016).
 [23] D. J. Singh, G. E. Jellison, and L. A. Boatner, Phys. Rev. B **74**, 155126 (2006).
 [24] K. Nomura, H. Ohta, A. Takagi, T. Kamiya, M. Hirano, and H. Hosono, Nature **432**, 488 (2004).
 [25] T. Kamiya, K. Nomura, and H. Hosono, Sci. Tech. Adv. Mater. **11**, 044305 (2016).
 [26] G. Kresse and J. Furthmüller, Phys. Rev. B **54**, 11169 (1996).
 [27] J. P. Perdew, J. A. Chevary, S. H. Vosko, K. A. Jackson, M. R. Pederson, D. J. Singh, and C. Fiolhais, Phys. Rev. B **46**, 6671 (1992).
 [28] J. P. Perdew, K. Burke, and M. Ernzerhof, Phys. Rev. Lett. **77**, 3865 (1996).
 [29] F. Tran and P. Blaha, Phys. Rev. Lett. **102**, 226401 (2009).
 [30] D. J. Singh, Phys. Rev. B **82**, 205102 (2010).
 [31] D. Koller, F. Tran, and P. Blaha, Phys. Rev. B **83**, 195134 (2011).
 [32] J. Heyd, G. E. Scuseria, and M. Ernzerhof, J. Chem. Phys. **118**, 8207 (2003).
 [33] J. Heyd, G. E. Scuseria, and M. Ernzerhof, J. Chem. Phys. **124**, 219906 (2006).
 [34] D. J. Singh and L. Nordström, *Planewaves, Pseudopotentials, and the LAPW method*, 2nd ed. (Springer, Berlin, 2006).
 [35] G. K. Madsen and D. J. Singh, Comput. Phys. Commun. **175**, 67 (2006).
 [36] Y. Wang, J. Lv, L. Zhu, and Y. Ma, Phys. Rev. B **82**, 094116 (2010).

- [37] Y. Wang, J. Lv, L. Zhu, and Y. Ma, *Comput. Phys. Commun.* **183**, 2063 (2012).
- [38] J. E. Medvedeva and C. L. Hettiarachchi, *Phys. Rev. B* **81**, 125116 (2010).
- [39] K. P. Ong, X. Fan, A. Subedi, M. B. Sullivan, and D. J. Singh, *APL Mater.* **3**, 062505 (2015).
- [40] Y. Li, L. Zhang, Y. Ma, and D. J. Singh, *APL Mater.* **3**, 011102 (2015).
- [41] V. V. Chernaya, A. S. Mitiaev, P. S. Chizhov, E. V. Dikarev, R. V. Shpanchenko, E. V. Antipov, M. V. Korolenko, and P. B. Fabritchnyi, *Chem. Mater.* **17**, 284 (2005).
- [42] M. Mathew, L. W. Schroeder, and T. H. Jordan, *Acta Crystallogr., Sect. B* **33**, 1812 (1977).
- [43] L.-Q. Fan, J.-H. Wu, and Y.-F. Huang, *Zeitschrift für anorganische und allgemeine Chemie* **634**, 534 (2008).

Supplemental Material for “Sn(II)-containing phosphates as optoelectronic materials”

Qiaoling Xu,¹ Yuwei Li,² Lijun Zhang,^{1,*} Weitao Zheng,¹ David J. Singh,^{1,2,†} and Yanming Ma^{3,‡}

¹*College of Materials Science and Engineering and Key Laboratory of Automobile Materials of MOE, Jilin University, Changchun 130012, China*

²*Department of Physics and Astronomy, University of Missouri, Columbia, MO 65211-7010 USA*

³*State Key Laboratory of Superhard Materials, Jilin University, Changchun 130012, China*

arXiv:1612.01372v1 [cond-mat.mtrl-sci] 5 Dec 2016

* lijun_zhang@jlu.edu.cn

† singhdj@missouri.edu

‡ mym@jlu.edu.cn

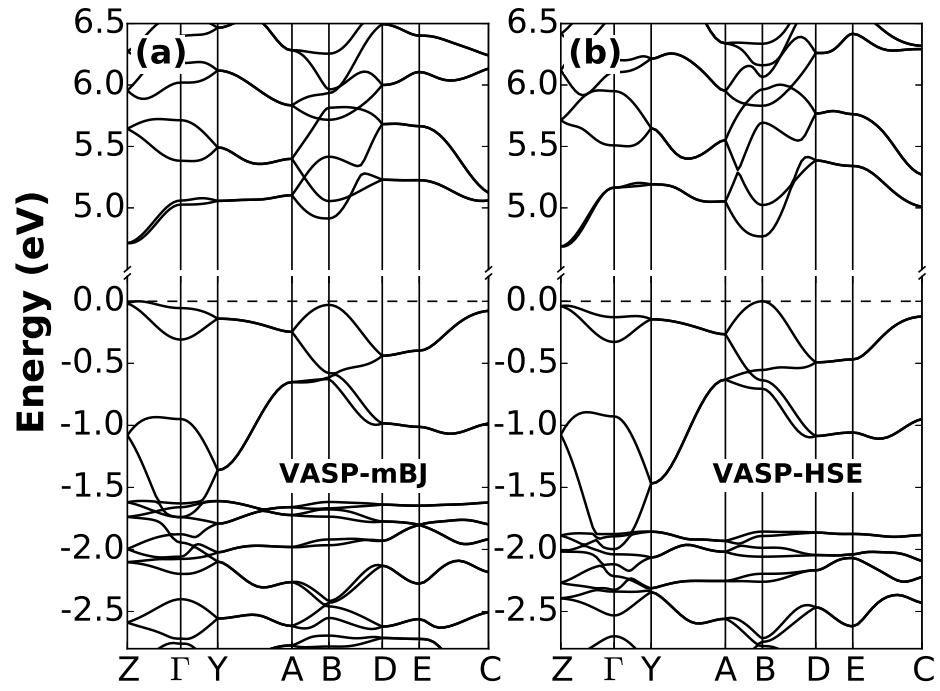


FIG. 1. (color online) Calculated electronic band structures of α - $\text{Sn}_2\text{P}_2\text{O}_7$ with different functionals: (a)VASP-mBJ, (b)VASP-HSE06.

TABLE I. Detailed structural information of predicted stable $\text{Sn}(\text{PO}_3)_2$.

Phase	Lattice parameters	Atomic coordinates (fractional)			
$\text{Sn}(\text{PO}_3)_2$ - Cc	$a=13.139 \text{ \AA}$	Sn (4a)	0.626	0.116	0.999
	$b=7.010 \text{ \AA}$	P (4a)	0.390	-0.103	0.551
	$c=10.618 \text{ \AA}$	P (4a)	0.575	0.376	0.372
	$\alpha=\gamma=90^\circ$	O (4a)	0.205	0.106	0.881
	$\beta=138.896^\circ$	O (4a)	0.534	0.429	0.880
		O (4a)	0.431	-0.308	0.650
		O (4a)	0.452	-0.057	0.189
		O (4a)	0.432	0.104	0.953
		O (4a)	0.621	0.221	0.505

TABLE II. Optimized lattice parameters (experiment in parenthesis) of the $\text{Sn}_n\text{P}_2\text{O}_{5+n}$ ($n=1-5$).

	$a(\text{\AA})$	$b(\text{\AA})$	$c(\text{\AA})$
n=1 ($\text{Sn}(\text{PO}_3)_2$)	13.139	7.010	10.618
n=2 (β - $\text{Sn}_2(\text{P}_2\text{O}_7)$)	5.420(5.277)	11.901(11.541)	11.966(11.636)
n=2 (α - $\text{Sn}_2(\text{P}_2\text{O}_7)$)	7.100(7.176)	9.770(9.287)	5.410(5.296)
n=3 ($\text{Sn}_3(\text{PO}_4)_2$)	11.457(11.092)	4.954(4.830)	16.845(16.405)
n=4 ($\text{Sn}_4\text{O}(\text{PO}_4)_2$)	7.512(7.353)	9.695(9.499)	14.271(13.716)
n=5 ($\text{Sn}_5\text{O}_2(\text{PO}_4)_2$)	7.316(7.174)	7.354(7.175)	13.363(12.895)